

# Low-temperature Synthesis of Large-area Films of Molybdenum Trioxide Microbelts in Air and the Dependence of their Field Emission Performance on Growth Conditions

Dongmei Ban, Ningsheng Xu+, Shaozhi Deng, Jun Chen and Juncong She

State Key Lab of Optoelectronic Materials and Technologies, Guangdong Province Key laboratory of Display Material and Technology, School of Physics and Engineering, Sun Yat-sen University, Guangdong, 510275, China

[Manuscript received 2009-3-24, in revised form 2009-7-28]

We demonstrate a simple method for preparation of large-area films of molybdenum trioxide ( $\text{MoO}_3$ ) microbelts. It is found that such films may be grown on ITO glasses or silicon substrates at low temperatures by thermal evaporation deposition in air without using catalyst. Field emission measurements show that the turn-on field of the  $\text{MoO}_3$  microbelts may be as low as 2.2 V/  $\mu\text{m}$  required to obtain a current density of 10 A/cm<sup>2</sup>. The combination of the simplicity of the growth method and the attractive field emission performance leads one to consider it as a potential low-cost technique for preparation of large-area field emission cold cathode material.

**KEY WORDS:** Field emission; Large-area film; Molybdenum trioxide; Microstructures and synthesis

## 1. Introduction

Molybdenum trioxide ( $\text{MoO}_3$ ) is an interesting photochromic and electrochromic material, attractive for information display, sensor device and smart window<sup>[1-6]</sup>. In addition, it is a good precursor for the synthesis of many other important materials, such as  $\text{MoS}_2$ ,  $\text{MoSe}_2$ , Mo, and host-guest compounds<sup>[7-10]</sup>. Recently the attractive field emission properties of  $\text{MoO}_3$  nanostructures such as nanoflowers<sup>[11]</sup>, nanowires<sup>[12,13]</sup> and

nanobelts<sup>[14]</sup> have been reported and thus they may be considered as potential cold cathode material applicable in field emission display<sup>[15]</sup>, lighting device<sup>[16]</sup> and plasma source<sup>[17]</sup>. In order to develop techniques for control growth, the synthesis method and the growth mechanism of  $\text{MoO}_3$  nanostructures have been a topic of investigation<sup>[11-14,18-22]</sup>. One issue is about how to prepare a large-area film of  $\text{MoO}_3$  nanostructures. Many related synthesis methods reported so far require vacuum conditions, and/or high growth temperature, and it will not be easy to develop these methods for preparation of large-area

---

+ Corresponding author. Prof., Ph.D.; Tel.: +86 20 84110916; Fax: +86 20 84037855; E-mail address: stsxns@mail.sysu.edu.cn (N.S. Xu).

film. In the present study, we investigated the possibility of growth of large-area MoO<sub>3</sub> microbelts on ITO glasses or silicon substrates at low temperature and without catalyst. The results reported here are in particular relevant to field emission display or smart windows.

## 2. Experimental

Our samples were prepared in a commercial infrared sintering furnace, which comprises 6 temperature zones. The length of each heating zone is 35 cm, and the width is 30 cm. The temperatures in each zone can be changed from room temperature to 1000°C. **Figure 1** illustrates the arrangement of sample and evaporation source for our present study. When the furnace is heated and reaches the set temperatures, the substrates and the quartz boat containing Mo powders are carried to the set zones by the transmission belt from the entrance. The source materials are placed in the high temperature zone and the substrate in the low temperature one. The materials, which vapor from the source, are deposited on the substrate since it has lower temperature. In our method, MoO<sub>3</sub> microbelts grow in air and do not involve the use of other protection gases. The advantages of using a commercial infrared sintering furnace include: (i) the substrate area can be very large; (ii) easy to change deposition temperatures using the combination of different temperature zones; (iii) uniformity in the temperature inside the furnace.

Our sample preparation procedure is as below. ITO glasses or silicon substrates were washed with acetone and then with alcohol in an ultrasonic cleaner. The temperatures of Zone 1 to 6 were set to 200°C, 200°C, 350°C, 700°C, 700°C and 100°C and heated, respectively. The substrate was placed in Zone 2 and the vapor source in Zone 5. They were then kept in their zones for 60 minutes. Finally, all the temperature zones were

allowed to decrease gradually to room temperature. The substrate appeared white after deposition.

The as-prepared products were characterized and analyzed by using X-ray diffraction spectroscopy (D/max 2200 vpc apparatus with Cu K radiation), scanning electron microscopy (SEM: Quanta 400F), and high-resolution transmission electron microscopy (HRTEM: JEM-2010HR).

## 3. Results and Discussion

### 3.1 Morphology and structure

For the present study, the as-prepared samples have an area of about 3 cm×3 cm. The SEM image in **Fig. 2(a)** shows that the MoO<sub>3</sub> microbelts exhibit a wide range of widths, ranging from 500 nm to 2 μm, with thickness of about 100 nm. The length of microbelts may exceed 10 μm (**Fig. 2(b)**). The XRD pattern of the MoO<sub>3</sub> microbelts is given in **Fig. 2(c)**, and the diffraction peaks can be indexed to the MoO<sub>3</sub> orthorhombic structure with the lattice parameters: a=3.96 Å, b=13.86 Å, c=3.7 Å (JCPDS: 5-0508). **Fig. 2(d)** is the low-magnification TEM image of the MoO<sub>3</sub> microbelts. The free end of a MoO<sub>3</sub> microbelt has been seen to have edges and corners, which may give electrical field enhancement useful to field emission. The high resolution TEM (HRTEM) image (**Fig. 2(e)**) shows the two sets of parallel fringes with a spacing of 3.96 Å and 3.7 Å corresponding to the (100) and (001) planes, respectively. The SAED patterns (inset, **Fig. 2(e)**) recorded perpendicular to the growth axis of a single MoO<sub>3</sub> microbelts is attributed to the [001] zone axis diffraction of orthorhombic MoO<sub>3</sub>. The HRTEM image also shows the existence of defects and the growth at low substrate temperature is the possible reason.

### 3.2 Growth mechanism

We assume that the growth mechanism follows a vapor-solid process, which is similar to the growth of MoO<sub>3</sub> nanowires reported early [12, 13]. The oxide vapor, evaporated from the starting oxide at a higher temperature zone, directly deposits on a substrate at a lower temperature region, resulting in the nucleation and growth by continuously receiving the incoming vapor. In order to understand how the MoO<sub>3</sub> microbelt is formed, we examine the anisotropy orthorhombic structure of MoO<sub>3</sub> (Fig. 2(f)). It illustrates in details the distorted octahedral configuration with a corner sharing in the direction of the a-axis (O (2) of the Fig. 2(f)), a zigzag edge sharing in the direction of the c-axis (O (3) of the Fig. 2(f)) and an unshared oxygen atom in b-axis (O (1) of Fig. 2(f)). For the orthorhombic MoO<sub>3</sub>, the (001) low-index surfaces are likely to have the lowest energy, and thus, the MoO<sub>3</sub> microstructures are likely to grow on (001) facets, which is a common phenomenon in the MoO<sub>3</sub> microstructures [12, 13, 18]. The substantial difference of the bonding configuration along [010] and [100] directions will have notably different ability of absorbing the incoming molecules of the source, leading to difference in growth rate [14], and thus, the MoO<sub>3</sub> microbelt forms.

### 3.3 Field emission property

The field emission measurements of the MoO<sub>3</sub> microbelts were carried out in a vacuum chamber of  $\sim 5.0 \times 10^{-7}$  torr at room temperature. The substrate with microbelts was first adhered to the surface of an oxygen-free, high-conductivity copper disc. A transparent anode, consisting of a quartz plate 4 cm in diameter and coated with conducting Indium doped tin oxide film, was placed in front of, and parallel to, the surface of the

sample cathode.

In order to find the optimal conditions for samples with high performance of field emission, we studied the dependence of their field emission characteristics on the growth duration. We found that the length and thickness of the MoO<sub>3</sub> microbelts were affected by growth duration. The SEM image of the MoO<sub>3</sub> microbelt films with different growth duration are shown as Fig. 3. The insets are the high resolution SEM images to show more details of the morphology of the MoO<sub>3</sub> microbelts. Figure 4 shows their field emission J-E and the corresponding F-N curves. It is obvious that a film having a higher aspect ratio has a lower turn-on field. The corresponding relationship may be seen in Table 1, which lists the length, the width and aspect ratio of each sample of different growth duration and the corresponding turn-on field. Their aspect ratios are about 1.3, 4, 6.7, and 10 corresponding to the growth duration of 1, 3, 10 and 60 min respectively. The best value of turn-on field is 2.2 V/  $\mu\text{m}$ , and is for the sample of the longest duration (60 min) and the highest aspect ratio (10). The turn-on fields from our samples of MoO<sub>3</sub> microbelts are found to be lower than that of the MoO<sub>3</sub> nanobelt (8.7 V/  $\mu\text{m}$  at 10 A/cm<sup>2</sup>)<sup>[14]</sup>, nanoflower (4.3 V/  $\mu\text{m}$  at 10 A/cm<sup>2</sup>)<sup>[11]</sup> and of MoO<sub>3</sub> nanowires (3.5 V/  $\mu\text{m}$  at 10 A/cm<sup>2</sup>) [12, 13], which were reported early. The results indicate that the MoO<sub>3</sub> microbelts are a good candidate as cold-cathode material. In addition, Fig. 5 shows the optical images of field emission site distribution for the different samples, and one may see that emission sites are distributed over the entire sample surface. Finally, the emission stability of our samples of MoO<sub>3</sub> microbelt was studied. Fig. 6 shows a typical field emission I-t curve recorded for 3 h at a constant electric field of 10.7 V/  $\mu\text{m}$  for an average emission current of 500. No

significant decrease of current was observed and the fluctuation was about 2%.

#### 4. Conclusion

We have demonstrated that large-area films of crystalline MoO<sub>3</sub> microbelts may be grown on ITO glasses or silicon substrates by thermal evaporation in air using a commercial infrared sintering furnace. This method is simple and can be of high yield. The MoO<sub>3</sub> microbelts are of orthorhombic structure with  $a=0.396$  nm,  $b=1.386$  nm,  $c=0.37$  nm, and the growth direction is [001]. By controlling the growth duration, films of MoO<sub>3</sub> microbelt with different aspect ratio may be prepared. The longer growth duration leads to longer length and higher aspect ratio of the MoO<sub>3</sub> microbelts, and the higher of their aspect ratio the lower their turn-on field is. The observed turn-on fields of our samples of MoO<sub>3</sub> microbelts are lower than MoO<sub>3</sub> nanobelts and nanowires previously reported. In addition, the films of MoO<sub>3</sub> microbelts are found to have stable field emission characteristic.

#### Acknowledgements

The authors gratefully acknowledge the financial support of the project from the National Natural Science Foundation of China (Grant No. U0634002, 50725206, 60571035 and 50672135), Science and Technology Ministry of China (National Basic Research Program of China: Grant No. 2003CB314701, 2007CB935501 and 2008AA03A314), the Science and Technology Department of Guangdong Province, the Department of Information Industry of Guangdong Province, and the Science and Technology Department of Guangzhou City.

#### REFERENCES

- [1] Y. Liu, Y. Qian, M. Zhang, Z. Chen and C. Wang: *Mater. Res. Bull.*, 1996, 31, 1029.
- [2] Z. Hussain: *J. Mater. Res.*, 2001, 16, 2695.
- [3] H. C. Zeng: *Inorg. Chem.*, 1998, 37, 1967.
- [4] J. N. Yao, K. Hashimoto and A. Fujishima: *Nature*, 1992, 355, 624.
- [5] L. Margulis, G. Salitra, R. Tenne and M. Talianker: *Nature*, 1993, 365, 113.
- [6] O. M. Hussain and K. S. Rao, *Mater. Chem. Phys.*, 2003, 80, 638.
- [7] M. Hershinkel, L. A. Gheber, V. Volterra, J. L. Hutchison, L. Margulis and R. Tenne: *J. Am. Chem. Soc.*, 1994, 116, 1914.
- [8] Y. Feldman, E. Wasserman, D. J. Srolovitz and R. Tenne: *Science*, 1995, 267, 222.
- [9] H. A. Therese, N. Zink, U. Kolb and W. Tremel, *Solid State Science*, 2006, 8, 1133.
- [10] M. Afsharpour, A. Mahjoub and M. M. Amini, *J. Inorg. Organomet. Polym.*, 2008, 18, 472.
- [11] G. D. Wei, W. P. Qin, D. S. Zhang, G. F. Wang, R. J. Kim, K. Z. Zheng and L. L. Wang: *J. Alloy Compd.*, 2009, 481, 417.
- [12] J. Zhou, S. Z. Deng, N. S. Xu, J. Chen and J. C. She: *Appl. Phys. Lett.*, 2003, 83, 2653.
- [13] J. Zhou, N. S. Xu, S. Z. Deng, J. Chen, J. C. She and Z. L. Wang: *Adv. Mater.*, 2003, 15, 1835.
- [14] Y. B. Li, Y. Bando, D. Golberg and K. Kurashima: *Appl. Phys. Lett.*, 2002, 81, 5048.
- [15] X. S. Fang, Y. Bando, U.K. Gautam, C. H. Ye and D. Golberg: *J. Mater. Chem.*, 2008, 18, 509.
- [16] J. Chen, X. H. Liang, S. Z. Deng, and N. S. Xu: *J. Vac. Sci & Tech. B*, 2003, 21, 1727.
- [17] A. Agiral, A.W. Groenland, J.K. Chinthaginjala, K. Seshan, L. Lefferts and J. G. E. H. Gardeniers: *J Phys. D: Appl. Phys.*, 2008, 41, 194009.
- [18] X. L. Li, J. F. Liu and Y. D. Li: *Appl.*

Phys. Lett., 2002, 81, 4832.

[19] L. F. Jiao, H. T. Yuan, Y. C. Si, Y. J. Wang, M. Zhao and Y. M. Wang: *Mater. Lett.*, 2005, 59, 3112.

[20] G. C. Li, L. Jiang, S. P. Pang, H. R. Peng

and Z. K. Zhang: *J. Phys. Chem. B*, 2006, 110, 24472.

[21] G. Wang, Y. Ji, L. H. Zhang, Y. M. Zhu, P. I. Gouma and M. Dudley: *Chem. Mater*, 200

### **Figures and table captions**

Table 1 Turn-on fields of the MoO<sub>3</sub> microbelt films of different aspect ratios

Fig. 1 Schematic diagram showing how substrate and evaporation source are arranged inside the furnace

Fig. 2 (a) typical SEM image (top view) of the MoO<sub>3</sub> microbelts and (b) the cross-section SEM image, (c) the typical XRD spectra of the MoO<sub>3</sub> microbelts, (d) the typical TEM image of MoO<sub>3</sub> microbelts and the HRTEM image is in (e) with the inset showing the corresponding SAED pattern, (f) illustration of atomic arrangement of the MoO<sub>3</sub> orthorhombic structure. The green balls represent atoms of Molybdenum, and the red balls correspond to the atoms of oxygen. The distorted octahedral is corner sharing in the direction of the a-axis (O (2)), zigzag edge sharing in the direction of the c-axis (O (3)) and unshared oxygen in b-axis (O (1))

Fig. 3 Scanning electron micrographs of MoO<sub>3</sub> microbelt films of different aspect ratios grown with different durations: (a) 1 min, (b) 3 min, (c) 10 min and (d) 60 min

Fig. 4 Field emission current density versus electric field (*J-E*) plots of MoO<sub>3</sub> microbelt films grown with different durations and their corresponding F-N plots (inset)

Fig. 5 Optical images of field emission site distribution of MoO<sub>3</sub> microbelt films of different aspect ratios grown with different durations: (a) 1 min, (b) 3 min, (c) 10 min and (d) 60 min

Fig. 6 The curve of field emission current versus time, showing good stability of field emission of the MoO<sub>3</sub> microbelt films

## Table list:

Table 1 Turn-on fields of the MoO<sub>3</sub> microbelt films of different aspect ratios

|          | Growth duration (min) | Length ( $\mu\text{m}$ ) | Width ( $\mu\text{m}$ ) | Aspect ratio | Turn-on field ( $\text{V}/\mu\text{m}$ ) |
|----------|-----------------------|--------------------------|-------------------------|--------------|--|
| Sample 1 | 1                     | 2                        | 1.5                     | 1.3          | 3.6                                      |
| Sample 2 | 3                     | 4                        | 1                       | 4            | 3.4                                      |
| Sample 3 | 10                    | 10                       | 1.5                     | 6.7          | 2.8                                      |
| Sample 4 | 60                    | 20                       | 2                       | 10           | 2.2                                      |

## Figure list:

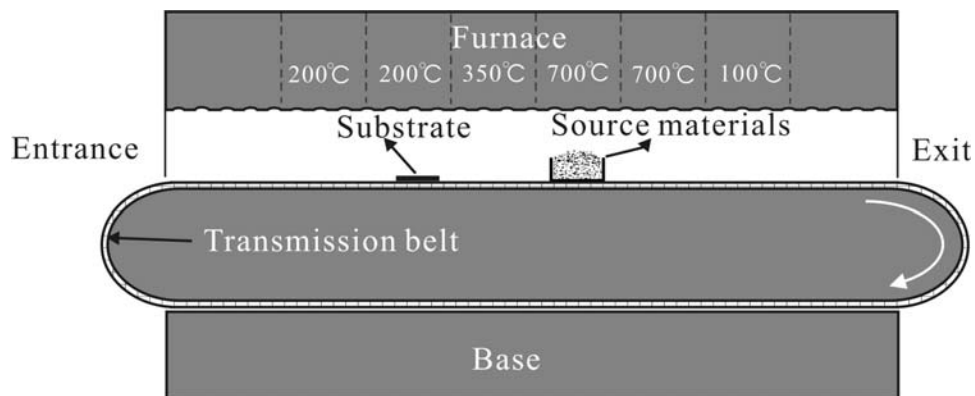


Fig. 1 Schematic diagram showing how substrate and evaporation source are arranged inside the furnace

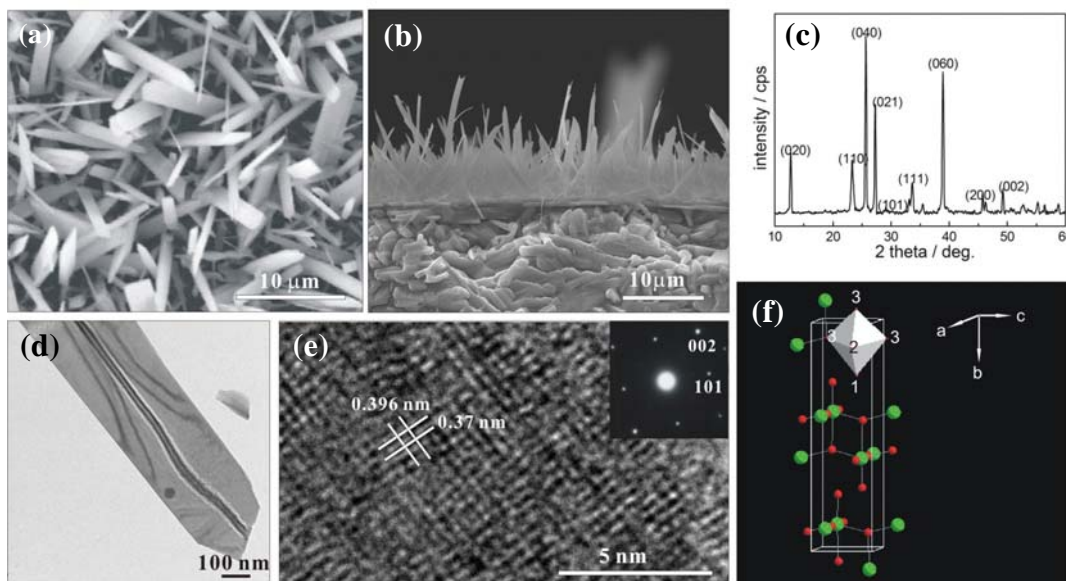


Fig. 2 (a) typical SEM image (top view) of the  $\text{MoO}_3$  microbelts and (b) the cross-section SEM image, (c) the typical XRD spectra of the  $\text{MoO}_3$  microbelts, (d) the typical TEM image of  $\text{MoO}_3$  microbelts and the HRTEM image is in (e) with the inset showing the corresponding SAED pattern, (f) illustration of atomic arrangement of the  $\text{MoO}_3$  orthorhombic structure. The green balls represent atoms of Molybdenum, and the red balls correspond to the atoms of oxygen. The distorted octahedral is corner sharing in the direction of the  $a$ -axis (O (2)), zigzag edge sharing in the direction of the  $c$ -axis (O (3)) and unshared oxygen in  $b$ -axis (O (1))

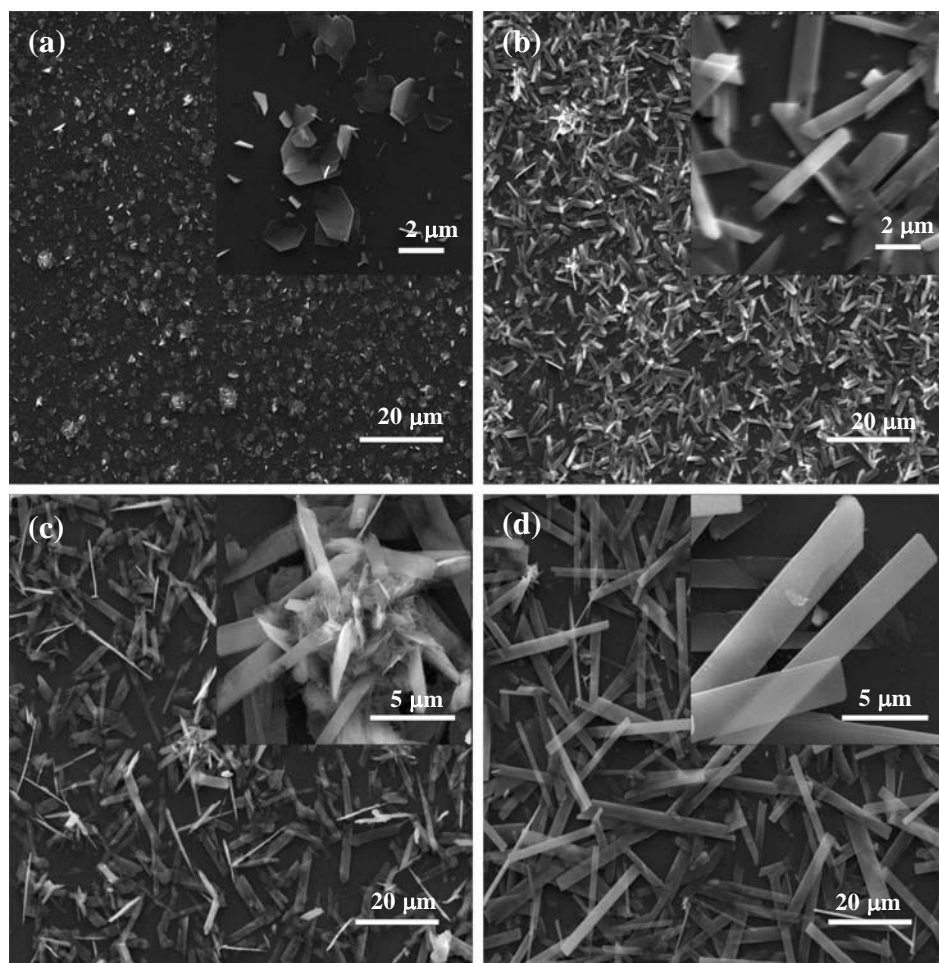


Fig. 3 Scanning electron micrographs of MoO<sub>3</sub> microbelt films of different aspect ratios grown with different durations: (a) 1 min, (b) 3 min, (c) 10 min and (d) 60 min

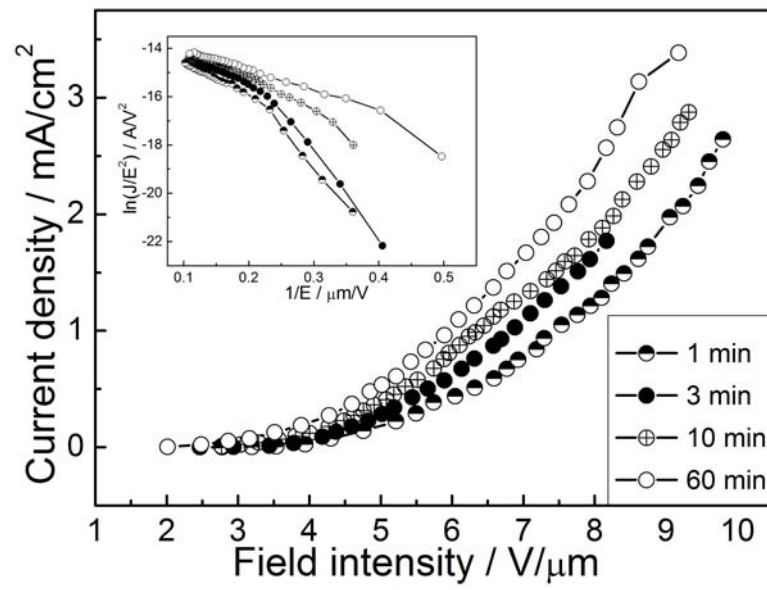


Fig. 4 Field emission current density versus electric field ( $J$ - $E$ ) plots of MoO<sub>3</sub> microbelt films grown with different durations and their corresponding F-N plots (inset)

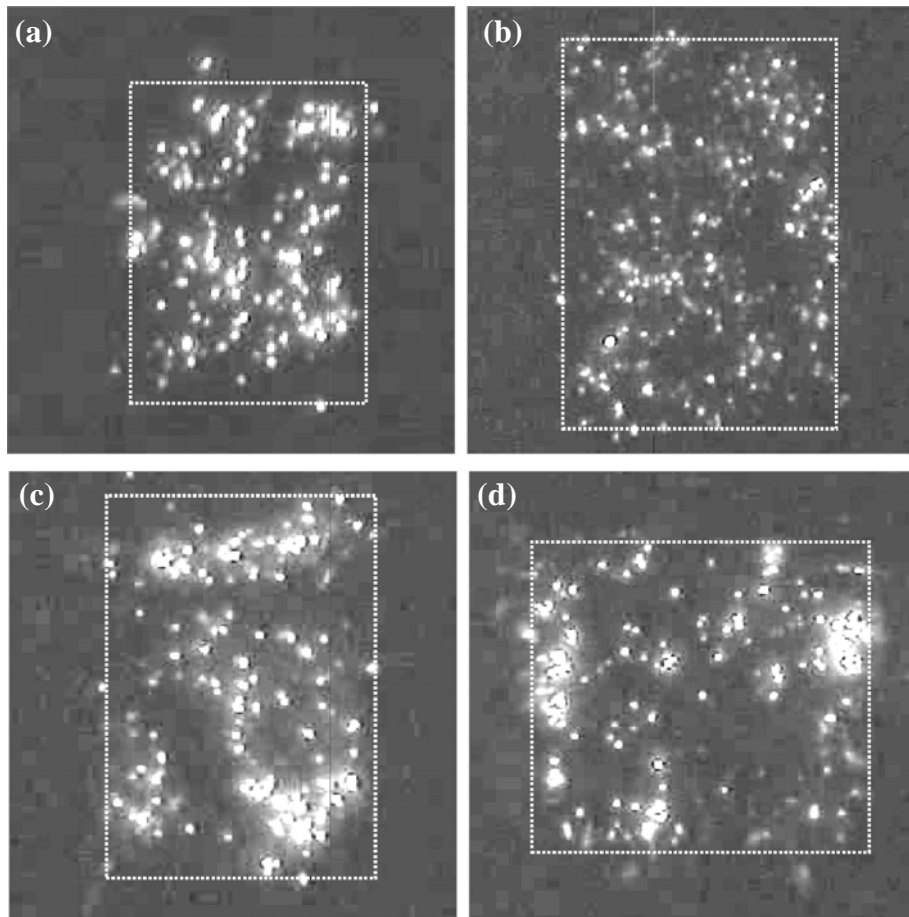


Fig. 5 Optical images of field emission site distribution of MoO<sub>3</sub> microbelt films of different aspect ratios grown with different durations: (a) 1 min, (b) 3 min, (c) 10 min and (d) 60 min

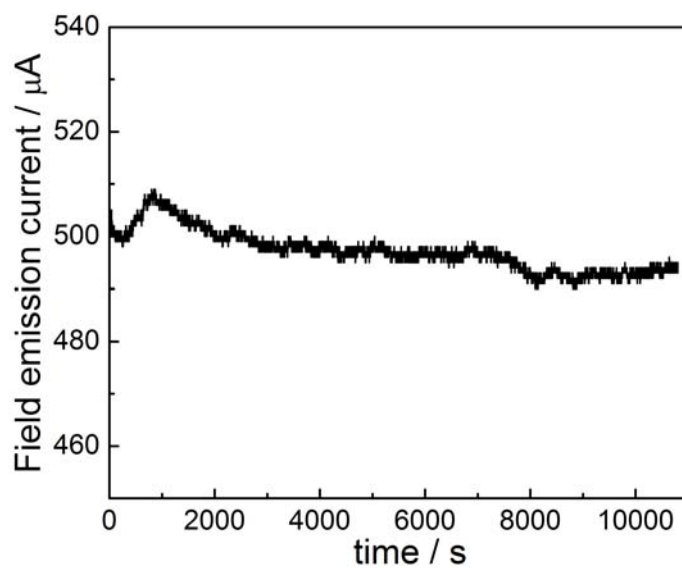


Fig. 6 The curve of field emission current versus time, showing good stability of field emission of the  $\text{MoO}_3$  microbelt films